Chemically dependent traps and polytypes at Pt/Ti contacts to 4H and 6H–SiC

S. Tumakha[a)]
Department of Physics, The Ohio State University, 174 West 19th Avenue, Columbus, Ohio 43210

L. J. Brillson
Department of Electrical Engineering, The Ohio State University, 205 Dreese Lab, Columbus, Ohio 43210-1272 and Department of Physics and Center for Materials Research, The Ohio State University, 174 West 19th Avenue, Columbus, Ohio 43210

G. H. Jessen
Department of Electrical Engineering, The Ohio State University, 205 Dreese Lab, Columbus, Ohio 43210-1272

R. S. Okojie
NASA-Glenn Research Center, 21000 Brookpark Road, M/S 77-1, Cleveland, Ohio 44135

D. Lukco
AYT 20001 Aerospace Parkway, Brookpark, Ohio 44142

M. Zhang and P. Pirouz
Case Western Reserve University, Cleveland, Ohio 44106

(Received 8 October 2001; accepted 28 December 2001)

We have used low energy electron-excited nanoluminescence (LEEN) spectroscopy and x-ray photoemission spectroscopy (XPS) to probe deep level defect states at interfaces of 4H and 6H–SiC with Ti/Pt metallization. These studies aim to identify process conditions under which thermally stable ohmic and Schottky contacts can be obtained on SiC while minimizing the formation of deep level electronic states. Depth-dependent LEEN measurements establish the presence of localized states and their spatial distribution on a nanometer scale. Spectra from the near interface region of 6H–SiC indicate the existence of a SiC polytype with a higher band gap of ~3.4 eV. Excitation of the intimate metal–SiC interface reveals a process-dependent discrete state deep within the SiC band gap. XPS measurements reveal consistent differences in the C 1*s* chemical bonding changes with specific process steps. Analogous chemical treatments of 4H–SiC also produce a lower band gap SiC polytype with ~2.5 eV energy extending tens of nanometers beyond the interface—confirmed by transmission electron microscopy. This work is the first to show the effect of metal–semiconductor interactions not only on localized states but also on the lattice structure of the semiconductor near the interface. [DOI: 10.1116/1.1451303]

I. INTRODUCTION

Silicon carbide (SiC) represents an excellent candidate for high-temperature electronic device applications because of its stability under harsh chemical and high temperature conditions. Although desirable ohmic or Schottky characteristics are obtainable for SiC devices, the interface properties depend significantly on specific process conditions used to prepare them. Localized electronic states at these interfaces are sensitive to such processing and can have substantial effects on barrier properties. However, relatively little is known about their properties compared with more conventional semiconductors.[1,2] Such states can be formed by the altered atomic arrangements and chemical bonding often present near interfaces. These could be localized just a few monolayers from the semiconductor/metal junction or buried a few nanometers or more below the interface. Hence, techniques with subsurface as well as surface sensitivity are required in order to probe such states.

The study of defect formation under controlled device processing conditions can be useful in understanding the origin of SiC interface states and the steps needed to minimize their density at electrical contacts. Furthermore, the polymorphic nature of SiC raises the possibility that structural relaxation, i.e., polytype phase transitions, can occur under certain conditions. Previously, it has been shown that phase changes may occur under applied stress[3,4] or high-temperature doping diffusion.[5] However, until now, there have been no studies of such changes with device processing or of their effect on interface transport properties. Titanium contacts to SiC are used generally to promote ohmic contact formation to single crystal SiC. Here we present results showing the effects of standard processing steps such as oxidation, HF strip, Piranha-clean and metallization on the formation of defect states and polytypic transformations near Pt/Ti/6H–SiC and 4H–SiC interfaces. After describing the experimental technique and processing in Sec. II, we will present results for interface states and structural changes of 6H–SiC and 4H–SiC in Secs. III and IV, respectively. Section IV also contains

a)Electronic mail: tumakha@mps.ohio-state.edu

TABLE I. Specimen surface process steps.

Step	Process
1	Acetone+methanol
2	4 h dry oxidation
3	HF strip, DI water rinse, and Piranha clean (*P* clean)
4	5 h dry oxidation at 1150 °C, HF strip, DI water rinse
5	Piranha clean (*P* clean)

results for extended polytype transformations at 4H–SiC surfaces and interfaces. Section V contains a discussion of our interface state results with those of previous studies. In addition, we show that the energies observed via low energy electron-excited nanoluminescence (LEEN) spectroscopy are consistent with the structural features evident in cross sectional tranmission electron microscopy (TEM) images as well as their quantum-confined properties. Section VI highlights the unique aspects of these SiC results relative to metal–semiconductor interface studies in general.

II. EXPERIMENT

All samples used for the LEEN analysis were processed and metallized at NASA-Glenn Research Center. In order to carry out optical studies on metal–SiC contacts, we used representative ohmic contact overlayers of Ti/Pt that were thin enough to transmit significantly in the visible wavelength region. Pt/Ti/6H–SiC and Pt/Ti/4H–SiC interfaces were formed by sputter deposition of 1–2 nm Ti followed by 2–3 nm Pt on chemically treated, SiC samples, all from the same wafer. The 6H–SiC wafers consisted of 2 μm thick, *n*-type ($N_d = 2\times10^{19}$ cm^{-3}) epilayers grown 3.5° off the basal (0001) plane on high resistivity *p*-type substrates by chemical vapor deposition. The 4H–SiC wafers consisted of 2 μm thick, *n*-type ($N_d = 1.7\times10^{19}$ cm^{-3}) epilayers grown 8° off the basal (0001) plane on high resistivity *p*-type substrates. All SiC wafers studied were supplied from Cree, Inc. Our studies followed the same sequence of process steps used conventionally to remove surface contamination and structural damage prior to ohmic contact formation. This sequence of process steps appears in Table I. First, the sample was cleaned with acetone and methanol. After this solvent clean, the sample was dry oxidized at 1150 °C for 4 h, after which the oxide was stripped with HF and the surface rinsed with de-ionized (DI) water. In order to remove any nonorganic contamination, the samples were then subject to a Piranha clean, consisting of 1:1 volume ratio of H_2SO_4 and H_2O_2 mixture. A subset of samples treated as above underwent a sescond dry oxidation, followed by a second HF strip and Pirhana clean (*P* clean). Finally, all specimes were metallized by the sputter deposition of Ti and Pt and prepared for LEEN. Sample sets that were treated similarly as above, but not metallized, were analyzed by x-ray photoemission spectroscopy (XPS) and TEM. We used LEEN luminescence spectroscopy, a low energy form of cathodoluminescence spectroscopy (CLS) to characterize the energies of electronic states as a function of distance from the SiC interfaces. This technique has provided similar information for a wide variety of semiconductor surfaces and interfaces.[6–10] Base pressure in the LEEN ultrahigh vacuum (UHV) chamber was 10^{-10} Torr. At NASA-Glenn, we performed monochromatized, Mg $K\alpha$ XPS measurements of chemical bonding changes in SiC core levels on similarly processed, but not metallized, samples. Also, similarly processed, but nonmetallized, samples were analyzed by TEM at Case Western Reserve University and NASA-Glenn. CLS and LEEN spectroscopy involve the excitation of electron–hole pairs by an incident electron beam. The electron beam generates a cascade of secondary electrons that lose energy to plasmons and subsequently electron–hole pair generation. The optical signal results from radiative recombination of these free electrons and holes. Energy loss in electron cascade and, therefore excitation depth varies with incident beam voltage E_B. This is illustrated by the inset in Fig. 1. The two curves in the main graph also illustrate changes in the maximum cascade penetration R_B beyond the free surface and the maximum excitation depth $U_0 \sim 1/3 R_B$. Both curves represent low energy approximations to polynomial expressions derived by Everhart and Hoff expressions and depend on incident beam energy E_B and material density.[11] These theoretical expressions agree with Monte Carlo simulations of backscattered electron trajectories that taken into account the different densities of metal versus SiC and the angle of incidence. At E_B of only a few hundred to several thousand volts, the Fig. 1 inset shows that the generation rate of electron–hole pairs

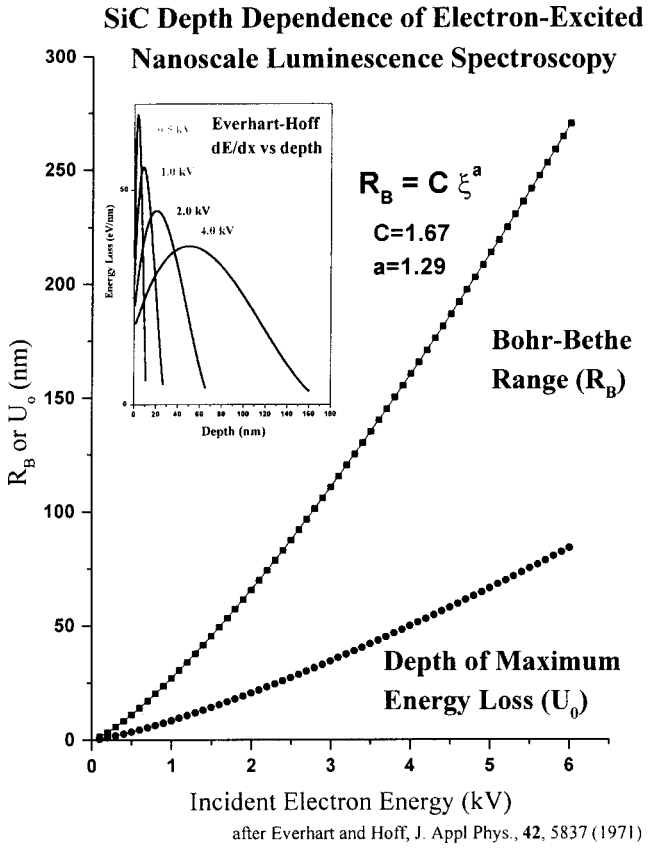

FIG. 1. LEEN depth–dose curve shows penetration depth vs E_B for SiC. Inset graph shows corresponding energy loss in cascade versus depth.

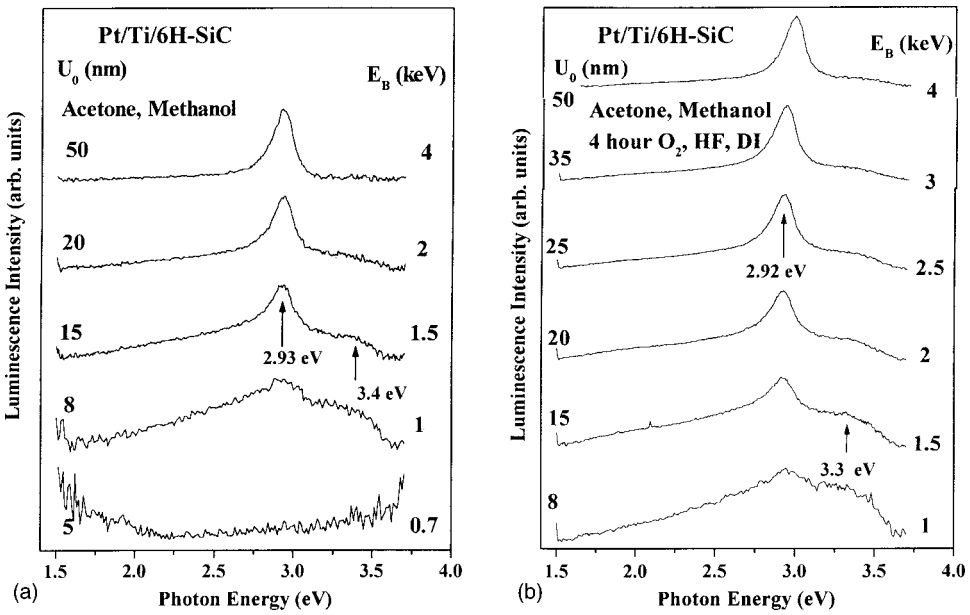

FIG. 2. LEEN spectra of 6H–SiC: (a) after acetone–methanol clean and metallization and (b) after acetone–methanol clean, 4 h dry oxidation, HF oxide strip, DI water rinse, and metallization. New phase formation is apparent near the interface in both cases.

peaks up in a depth range of nanometers. For example, with $E_B=1$ keV in SiC, $R_B=20$ nm and maximum excitation is at $U_0=8$ nm. This nanoscale excitation permits one to selectively probe the semiconductor from the interface to the bulk. Particularly in the surface-sensitive regime, LEEN spectra must be acquired in UHV in order to prevent contamination and signal deterioration due to associated nonradiative transitions and rapid deterioration of radiative transitions close to the surface.

III. 6H–SiC RESULTS

LEEN spectroscopy provided information on the energies and spatial depth distribution of localized states near the SiC–metal interfaces. Figure 2 illustrates two families of LEEN spectra taken with increasing E_B and peak excitation depth U_0. The spectra in Fig. 2(a) represent a depth profile corresponding to 6H–SiC after a methanol–acetone clean and subsequent Pt/Ti metallization The higher E_B spectra corresponding to the bulk ($U_0>25$ nm) display the characteristic 2.9 eV near band edge (NBE) emission of the 6H–SiC polytype. For comparison, Fig. 2(b) represents a depth profile corresponding to 6H–SiC after a methanol–acetone clean, a 4 h oxidation at 1150 °C followed by HF strip and DI water rinse, and a subsequent Pt/Ti metallization. Again, the higher E_B spectra display the characteristic 6H–SiC polytype emission at 2.9 eV. Similarly, Figs. 2(a) and 2(b) show additional features at 3.3 eV for the lower E_B spectra corresponding to the interface region ($U_0<20$ nm). Since these features have energies above the 6H–SiC band edge, they cannot be due to defect emission to or from states in the band gap. They are instead attributed to broken 6H lattice periodicity and polytype variation near the interface. Also near the interface, both Figs. 2(a) and 2(b) shows emission corresponding to a broad continuum of states below the band gap.

Figure 3 illustrates the depth-dependent LEEN features of the same surface following the *P*-clean step. Similar to Fig. 2, the 6H–SiC NBE feature at 2.9 eV dominates in the bulk, and the 3.3 eV local polytype feature is apparent near the interface. In addition, a 1.9 eV feature appears just below the metal/semiconductor interface. Note that 4 nm is the approximate metal overlayer thickness so that most electron excitation occurs within the metal layer. This variation in local electronic features near the interface is illustrated in Fig. 4 for an entire sequence of process steps. Features at 2.9 and 3.3 eV and the continuum of states are relatively independent of surface treatment before metallization. The 1.9 eV feature first appears after the first oxidation step, then increases after *P*-cleaning. Significantly, it is not observed

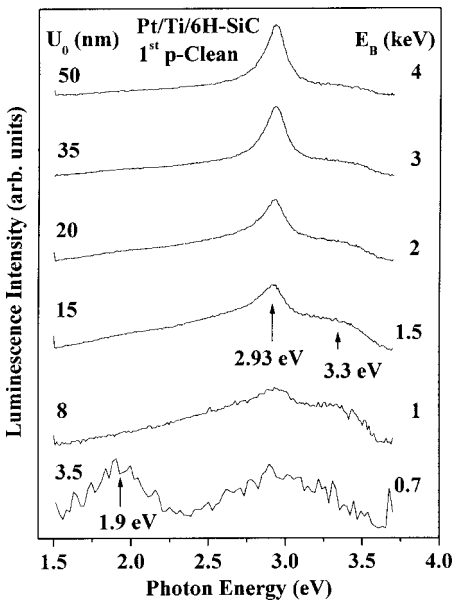

FIG. 3. LEEN spectra of 6H–SiC after Piranha clean reveal new defect formation near the interface.

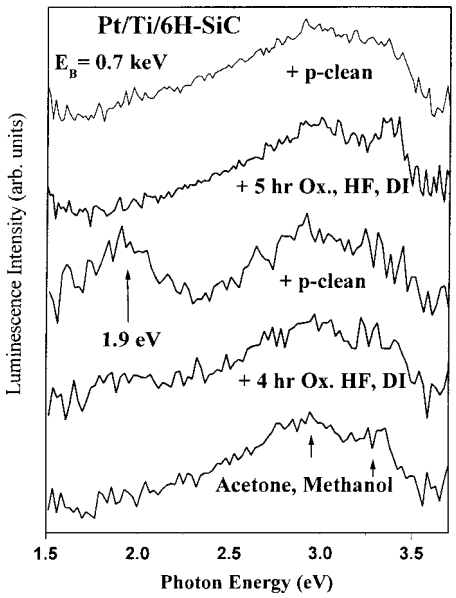

FIG. 4. LEEN spectra of 6H–SiC spectra directly under the metal show that 1.9 and 3.3 eV features are relatively independent of process, in contrast to the 1.9 eV feature that appears after the first *p* clean.

after the second oxidation, strip, and rinse, or the second *P* clean.

XPS spectra of the bare (no metallization) 6H–SiC surface after different process steps appears in Fig. 5. Here, C 1*s* core level peaks exhibit a dominant peak corresponding to bulk SiC and a smaller shoulder corresponding to near-surface C with higher binding energy. The near-surface spectrum after acetone and methanol rinse (diamonds) exhibits pronounced secondary C 1*s* intensity that is reduced almost completely (squares) by the first oxidation, HF strip, and DI water rinse. This spectrum indicates that oxidation/strip removes carbon with bonding different from the SiC bulk. Piranha cleaning on the surface (triangles) reduces the C 1*s* sideband and the second oxidation, HF strip, and DI rinse (*x* symbols) again reduces its intensity. Finally, the second *P* clean (* symbols) produces no significant change. Assuming that the C 1*s* peak is indicative of surface states, then the reduction in the higher binding energy C 1*s* peak with oxidation is consistent with removal of adventitious C and any lattice damage.

The depth dependence of interface and bulk features shown in Figs. 2 and 3 is consistent with TEM cross sectional images of the Ti/6H–SiC interface. The TEM image in Fig. 6 for sputtered a 100 nm Ti film on 6H–SiC (not part of the sequence above) exhibits sixfold periodicity characteristic of 6H–SiC layer stacking in the bulk semiconductor (right side). The periodicity of the deposited Ti's crystal structure is apparent to the left of the interface. Within the interface region, the disruption of 6H periodicity and possible formation of other polytypic phases is apparent. Significantly, the ~5 nm width of this disrupted interface agrees qualitatively with the ~15–10 nm total depth beyond the ~4 nm metal thickness into the SiC over which the 3.3 eV and continuum of gap states are predominant.

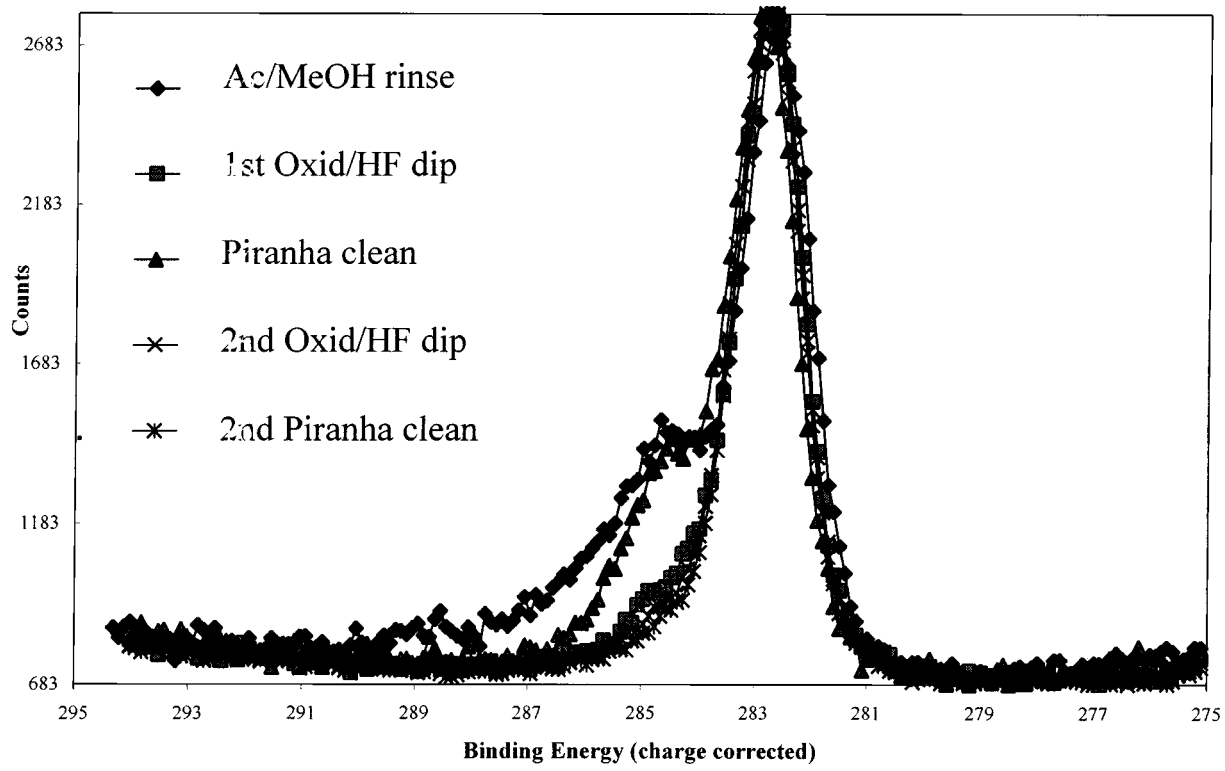

FIG. 5. XPS spectra of 6H–SiC surface treated after different process steps. The higher binding energy should corresponds to higher chemical bond strength than that in bulk SiC.

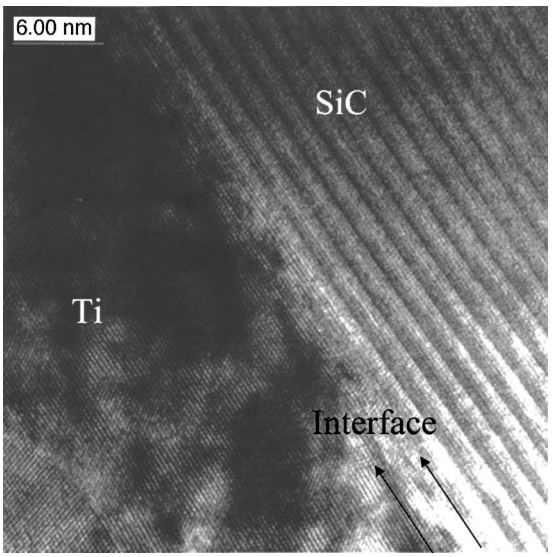

FIG. 6. TEM of a sputtered titanium (100 nm) on 6H–SiC shows broken 6H periodicity in the interface region on a scale of ~5 nm.

IV. 4H–SiC RESULTS

The LEEN spectral data for 4H–SiC yielded evidence for both localized states near the metal interface as well as a polytype transformation that extends at least 50 nm into the 4H–SiC bulk. Figure 7 illustrates depth-dependent LEEN spectra for a 4H–SiC sample after acetone and methanol cleaning. Analogous to the 6H–SiC results, we observe a mostly 4H band gap peak at 3.2 eV for E_B corresponding to bulk excitation. Similarly, as E_B decreases and excitation occurs closer to the interface, we observe additional emission at 3.4 eV and a broad continuum of states below the band gap energy. Figure 8 shows the spectra for 4H–SiC following the same 4 h, 1150 °C oxidation, HF strip, and DI water rinse as used with 6H–SiC in Fig. 2(b). For the 4H case, this process step introduces a dramatic change. Instead of increasing with increasing probe depth, the 4H–SiC NBE peak at 3.2 eV actually decreases. Furthermore, a new peak appears at 2.5 eV that increases with excitation depth and dominates the spectra in the bulk. The appearance of this peak suggests the formation of a 3C polytype, whose band gap is 2.39 eV at room temperature.[12] In addition, a broad spectral feature appears at ~2.0 eV with strong intensity for depths extending 20 nm in the bulk. Analogous to Figs. 2, 3, and 7, the interface region exhibits emission at ~3.3–3.4 eV as well as broad continuum of states below the band gap.

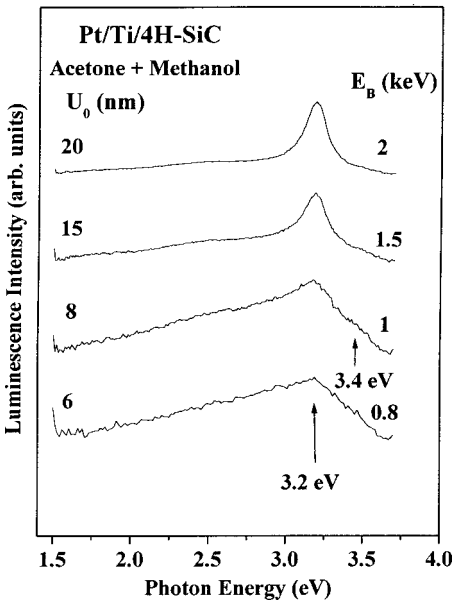

FIG. 7. LEEN spectra of 4H–SiC prior to oxidation showing only 3.2 eV NBE peak dominant at bulk excitation energies and higher energy features at 3.4 eV near interface.

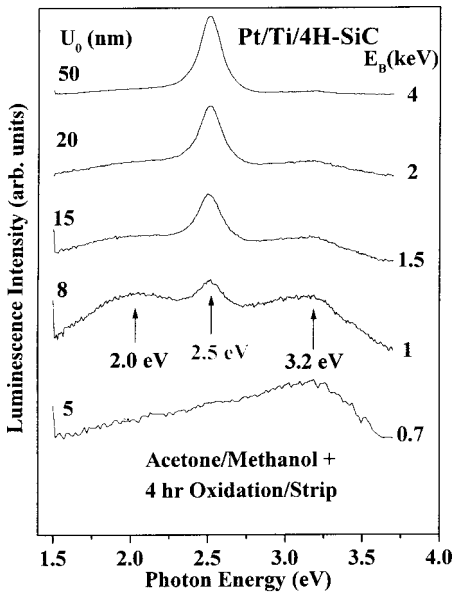

FIG. 8. LEEN spectra of 4H–SiC after oxidation showing the appearance of a 2.5 eV NBE emission due to 3C–SiC and the near disappearance of the 3.2 eV 4H–SiC NBE emission at all excitation depths. Multiple scans at certain E_B illustrate the spectral variability.

In order to confirm the appearance of a new polytype phase within the 4H–SiC bulk, we obtained TEM images of the 4H–SiC sample before and after oxidation. TEM images of 4H–SiC before oxidation show only the undistributed bulk crystal. In contract, Fig. 9 illustrates an image following oxidation. Here, 3C bands are evident in narrow bands running parallel to the basal plane, interchanging with 4H–SiC layers and extending deep in the bulk. The thickness of these 3C layers ranges from two 3C lattice repeat distances to several nanometers. Figure 9 displays sets of discrete transformation bands (DTBs), each containing multiple alternating bands of 3C– and 4H–SiC. In turn, these DTBs appear to be spaced several hundred nm apart and extend throughout the thickness of the epitaxial SiC layer. Nitrogen dopant redistribution is not detected by secondary ion mass spectroscopy, nor is Si or C precipitation detected by Auger electron spectroscopy, indicating no stoichiometric hange in the Si/C ratio.

V. DISCUSSION

The interface electronic properties of 6H–SiC LEEN spectra are consistent with previous measurements of

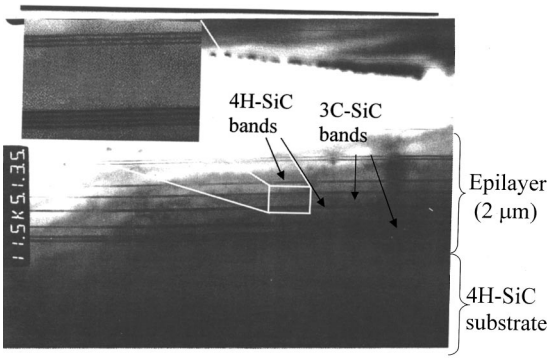

FIG. 9. TEM cross section after 4 h oxidation at 1150 °C shows 3C planar bands interchanged with 4H bands. Each of 3C bands is from two to several 3C unit cell heights thick.

Schottky barrier formation as well as with the XPS measurements of core level bonding. The 1.9 eV feature can be attributed to electronic states near midgap introduced by the Piranha cleaning. Fermi level ''pinning'' by discrete states located 1.9 eV below the conduction band edge would contribute to *n*-type Schottky barriers of the same energy. Previous work[13,14] indicated Fermi level positions 1.8–2.0 eV above the valence band edge for Ti on *n*-type 6H–SiC. The correspondence with the 1.9 eV emission provides modest evidence for the midgap state contributing to Fermi level pinning. Alternatively, this 1.9 eV emission may be due to incomplete silicon dioxide removal after oxidation or an oxide layer introduced by Piranha cleaning since a similar peak is found in studies of SiO_2 defects.[15] This is unlikely since such a defect is usually accompanied by comparable or stronger emission of an even more common SiO_2 feature at 2.7 eV,[15] that is not obvious from these 6H–SiC spectra. The introduction of the 1.9 eV LEEN feature by *P*-cleaning coincides with the appearance of additional C 1*s* core level emission at higher binding energy associated with new carbon bonding sites. Its absence for *P*-cleaning after the second oxidation suggests that lattice damage and/or contamination removed by the second oxidation and strip may contribute to such states as well. The continuum of states within the band gap at the metal interfaces of both 6H–SiC and 4H–SiC is consistent with a disordered interface and a distribution of localized states.[16] The agreement between the depth range of the 3.3 eV LEEN peak feature and the width of the Ti/6H–SiC interface confirms the surface sensitivity and nanoscale discrimination of depth-variable features electronic transitions using this technique. Furthermore, the presence of the 1.9 eV mid-gap states, the continuum of gap states, as well as the new polytype evidenced by 3.3 eV emission imply several different factors that can significantly affect the Schottky barrier formation.

In Fig. 8, the appearance of a pronounced peak feature at 2.5 eV following the oxidation process step indicates a conversion of the 4H–SiC polytype to 3C–SiC. Lattice images similar to the cross sectional TEM micrographs in Fig. 9 with atomic scale resolution display the characteristic 3C stacking sequence. Such transformation bands may be the result of lattice strain in the epilayer and the subsequent formation of stacking faults. Polytype transformations have been reported for 6H–SiC subjected to mechanical stress,[3,17] and electrical stress has been shown to produce stacking faults near metal contacts to 4H–SiC[18] and 6H–SiC.[19] for the 4H–SiC studied here, such stress may result from impurity-induced lattice mismatch between the epilayer and substrate. The discrepancy in energy between the observed 2.5 eV peak and the usual bulk value of 2.39 eV can be accounted for by the confined nature of 3C inclusions. Figure 9 and other TEM[20] images show that the thickness of the cubic 3C–SiC layers range from two 3C lattice parameters to many lattice parameters. The lowest thickness is most common and corresponds to a single stacking fault in the 4H–SiC lattice structure. At thicknesses of only a few nanometers, the conduction and valence band states can be described as quantum-confined states with new quantized energy state at the 3C/4H heterojunction that increase the NBE energy of recombination. In order to determine the transition energies associated with such confined states, we first calculated band offsets between 3C–SiC and 4H–SiC by comparing band offsets for 3C–SiC versus 6H–SiC[21] and 4H–SiC versus 6H–SiC.[22] This provides a cumulative 3C–SiC versus 4H–SiC conduction band offset value of $\Delta E_C = 0.84 \pm 0.1$ eV and a valence band offset value $\Delta E_V = 0.07 \pm 0.1$ eV. Here, the conduction band of 3C–SiC lies lower in energy than that of 4H–SiC, whereas the valence bands almost align. In this case, the positive conduction band offsets result in quantum wells for electrons inside the 3C band but no confinement for holes. For a quantum well of width 1.75 nm, corresponding to two 3C unit cell repeat distances normal to the basal plane, the lowest energy state for electrons with $m_{\text{eff}} = 0.66 m_0$[12] equals 0.11 eV from bottom of the well. Note that a ± 0.2 eV error in ΔE_C produces $<5\%$ change in this ground state energy. Also, the energy associated with any hole confinement is negligible. NBE emission in this structure would involve recombination of holes from the lowest quantum well (QW) state in the conduction band to the top of the valence band. The resulting emission would occur at: 2.39 eV (3C–SiC band gap) + 0.11 eV (QW ground energy state) = 2.5 eV. This results is in excellent agreement with the LEEN spectra. Furthermore, since the joint density of states of the 3C–SiC QW is higher than that of bulk 4H–SiC and the QW is an efficient collector of free electrons, the latter serves as a more efficient source of carrier recombination. This accounts for the much stronger 3C–SiC NBE emission relative to that of 4H–SiC in Fig. 8.

The ultrathin nature of the 3C–SiC layers embedded in 4H–SiC and the expected 3C–SiC band offsets indicate that these inclusions will form multiple quantum wells, and would therefore have a significant effect on Schottky barrier and ohmic contact properties. This is an unanticipated result, namely that standard device process steps can change the electronic and crystalline structure of conventional 4H–SiC. Structural changes observed in 4H–SiC Ti/Pt contacts manifest themselves in metal–4H–SiC current–voltage (I–V) measurements. Pt/Ti contacts to untransformed 4H–SiC ex-

hibit rectifying behavior, whereas the same metals on transformed 4H–SiC show a linear $I-V$ characteristic.[23] The control of such 4H to 3C conversion presents a challenge for current SiC microelectronics fabrication. Conversely, this finding opens the possibility for structures that take advantage of the band gap changes and quantum-scale confinement induced by the transformation.

VI. CONCLUSIONS

We have observed optical emission from discrete and continuum defect states on 6H–SiC/metal interfaces below the band gap and polytypic features above the band gap. The relative concentration of such features increases with proximity to the interface on a scale of nanometers. XPS core level spectra exhibit chemically shifted C binding energies consistent with the different process tseps and the changes in LEEN spectral features. TEM confirmed our results for polytypic formation within few nanometers from the interface. Analogous to 6H–SiC, 4H–SiC/metal interfaces displayed optical emission from discrete and continuum defect states, again increasing within a few nm of the interface. In contrast to 6H–SiC, 4H–SiC exhibits a pronounced polytype change to cubic 3C–SiC not only at the interface but extending hundreds of nm into the bulk. TEM cross sectional micrographs confirm the appearance and spatial extent of this 3C–SiC polytype transformation, revealing the presence of altenating layers of 3C–SiC and 4H–SiC in discrete transformation bands. These results have significant implications for the design and fabrication of SiC electronic devices.

[1]M. J. Bozack, Phys. Status Solidi B **202**, 549 (1997).
[2]H. Morkoc, S. Strite, G. B. Gao, M. E. Lin, B. Sverdlov, and M. Burns, J. Appl. Phys. **76**, 1363 (1994).
[3]Y. Yang and P. Pirouz, J. Mater. Res. **8**, 2902 (1993).
[4]A. V. Samant and P. Pirouz, Int. J. Refract. Met. Hard Mater. **16**, 277 (1998).
[5]J. Pezoldt, Mater. Sci. Eng., B **29**, 99 (1995).
[6]L. J. Brillson, H. W. Richter, M. L. Slade, B. A. Weinstein, and Y. Shapira, J. Vac. Sci. Technol. A **3**, 1011 (1985).
[7]L. J. Brillson, J. Vac. Sci. Technol. A **6**, 1437 (1988).
[8]L. J. Brillson, T. M. Levin, G. H. Jessen, and F. A. Ponce, Appl. Phys. Lett. **75**, 3835 (1999).
[9]A. P. Young and L. J. Brillson, Appl. Phys. Lett. **77**, 699 (2000).
[10]L. J. Brillson, J. Vac. Sci. Technol. B (in press).
[11]T. E. Everhart and P. H. Hoff, J. Appl. Phys. **42**, 5837 (1971).
[12]*Properties of Silicon Carbide*, edited by G. L. Harris (INSPEC, Institute of Electrical Engineers, London, 1995).
[13]J. R. Waldrop and R. W. Grant, Appl. Phys. Lett. **62**, 2685 (1993).
[14]H.-J. Im, B. Kaczer, and J. P. Pelz, Appl. Phys. Lett. **72**, 839 (1998).
[15]J. Schäfer, A. P. Young, L. J. Brillson, H. Niimi, and G. Lucovsky, Appl. Phys. Lett. **73**, 791 (1998).
[16]H. Hasagawa and H. Ohno, J. Vac. Sci. Technol. B **4**, 1130 (1986).
[17]P. Pirouz and J. W. Yang, Ultramicroscopy **51**, 189 (1993).
[18]J. P. Bergmann, H. Lendenmann, P. Å. Nilsson, U. Lindefelt, and P. Skytt, Mater. Sci. Forum **355–356**, 299 (2001).
[19]R. E. Stahlbush and P. J. MacFarlane, J. Electron. Mater. **30**, 188 (2001).
[20]R. S. Okojie, M. Xhang, P. Pirouz, S. Tumakha, G. Jessen, and L. Brillson, Appl. Phys. Lett. **79**, 3056 (2001).
[21]K. F. Dombrowski, U. Kaufman, M. Kunzer, K. Maier, J. Schneider, V. B. Shields, and M. G. Spencer, Appl. Phys. Lett. **65**, 1811 (1994).
[22]A. O. Evwaraye, S. R. Smith, and W. C. Mitchel, Appl. Phys. Lett. **67**, 3319 (1995).
[23]R. S. Okojie, M. Xhang, P. Pirouz, S. Tumakha, G. Jessen, and L. J. Brillson, Mater. Sci. Forum (in press).